The potential value of seasonal forecasts in a changing climate

H. C. Winsemius[1], E. Dutra[2], F.A. Engelbrecht[3,4], E. Archer Van Garderen[3,4], F. Wetterhal[2], F. Pappenberger[2,6], M. G. F. Werner[1,5]

[1] Deltares

[2] European Centre for Medium-Range Weather Forecasts

[3] Council for Scientific and Industrial Research

[4] School of Geography, Archaeology and Environmental Sciences, University of the Witwatersrand, South Africa

[5] UNESCO-IHE

[6] College of Hydrology and Water Resources, Hohai University, Nanjing, China

S1. Effect of climate change on dry spell and heat stress frequency

The effect of climate change on dry spell and heat stress frequency has been computed for a number of thresholds (dry spells of 3, 5 and 10 days, days with THI values of 72, 78 and 84). The main sections show only the dry spells of 5 days and days with THI of 78. In this supplementary material section we also show the results for the remainder of dry spell and THI thresholds. Figure S1 until Figure S4 show these results for the dry spells, Figure S5 until Figure S8 show the results for the THI conditions. The results clearly support that also for other thresholds than the ones presented in the main sections, the same conclusions can be drawn: dry spell frequencies are not clearly increasing in a changing climate, the current variability in dry spell frequency is much larger than its expected change. The frequency of heat stress conditions clearly increases. It can further be noted that extreme stress conditions with THI values above 84 are extremely rare in the current climate, but towards 2100 such conditions will occur quite frequently across low-lying areas such as the Zambezi delta and the Kalahari Desert (i.e. yellow coloured areas in the right-hand panes of Figure S6).

S2. Climatology of the indicator-threshold combinations

Figure S9 and S10 show (similar to Figure 4 and 5) the climatology of the indicator-threshold combinations that were not explicitly shown in the main materials: the frequency of dry spells of 3 days, and frequency of days with THI >= 72. Figure S11 shows the time series of these two indicator-threshold combinations, in analogue with Figure 6 in the main materials.

S3. Forecast skill scores calculation and uncertainty

The following points describe the scores used in the evaluation of the seasonal forecast skill and its uncertainty estimates.

Correlation maps (Figure S12 to Figure S15)

The correlation maps display the temporal grid-point correlation between two time series (forecast and verification) calculated as the ratio between the covariance of the two variables and the product of their standard deviations. In these calculations, it was not necessary to remove the mean (or mean annual cycles) since the time-series consist of yearly values (mean over the December-January period). The confidence intervals of the sample correlation coefficient were calculated using the Fisher transformation to determine if the correlations were statistically significantly different from zero. The grid-point correlations are only indicative, since we cannot expect to have detailed seasonal forecasts on the grid-point scale

Relative Operating Characteristic (ROC) scores (Figure 7, Figure S16, Table 1 and Table 2) and diagrams (Figure 8, Figure S17 and Figure S18)

ROC measures the skill of probabilistic categorical forecast, while the correlation (previous point) only considers the ensemble mean. The ROC diagram (Mason and Graham, 1999) displays the false alarm rate (FAR) as a function of hit rate (HR) for different thresholds (i.e. fraction of ensemble members detecting an event) identifying whether the forecast has the attribute to discriminate between an event or not. The area under the ROC curve is a summary statistic representing the skill of the forecast system. The area is standardized against the total area of the figure such that a perfect forecasts system has an area of 1 and a curve lying along the diagonal (no information) has an area of 0.5. The results presented in the manuscript refer to the Limpopo basin. This was achieved by using all the grid-points in the basin when calculating the contingency tables for the FAR and HR estimates. The forecasts and verification fields were transformed into an event (or no event) based on underlying grid-point distributions. This spatial integration has the advantage of increasing the sample size used to build the contingency table while no spatial information is retained.

To estimate the uncertainty of the ROC scores and the curves in the ROC diagram a 1000 bootstrap re-sampling procedure was applied. The contingency tables and the ROC scores were calculated 1000 times by temporal re-sampling: in each calculation the original forecast and verification grid-point time series are randomly replaced (allowing repetition) and a new set of scores is calculated. The re-sampling was performed only on the time-series, keeping all the grid-points, since the temporal sampling (in our case only 30 values) is the largest source of uncertainty in the scores estimation. The 95% confidence intervals are estimated from the percentiles 2.5 and 97.5 of the 1000 ROC values (and HIT, FAR).

Reliability diagrams (Figure 8, Figure S17 and Figure S18)

The reliability diagram (Hartmann et al., 2002) measures the consistency between predicted probabilities of an event and the observed relative frequencies. The diagram displays the observed frequency of an event plotted against the forecast probability of an event. Similarly to the ROC diagrams the REL diagrams are also applied to categorical forecasts. With a perfect forecast the REL diagram will lay over the diagonal, while curves with higher (lower) slopes indicate under-confident (over-confident) forecasts. The estimation of the confidence intervals followed the same 1000 bootstrap re-sampling procedure described above for the ROC scores.

S3. Forecast skill results

The forecast skill assessment has been performed on the frequency of dry spells of 3 days and 5 days, and frequency of days with THI larger than 72 and 78. In the main material only the dry spell frequency of 5 days, and THI frequency of 78 are presented, because these are most meaningful to end users. In this supplementary material the results for the remaining indicators are presented. The main results discussed for the indicator presented in the manuscript are reflected in the remaining indicators. In Figures S9 and S10, also the climatologies for dry day frequencies of 3 days and THI frequency of 72 are shown. The results show a similar pattern as the results with dry spells of 5 days and THI larger than 78, i.e. S4 is colder and/or drier than ERA-Interim (reflecting on THI frequency) with increasing lead time, and has a similar climatology for dry spells. S11 also shows the time series of the same indicator-threshold combinations, averaged over the Limpopo, and combined with the evolution of the RCMs in the current and future (2079-2100) climate.

References

Hartmann, H. C., Pagano, T. C., Sorooshian, S. and Bales, R.: Confidence Builders: Evaluating Seasonal Climate Forecasts from User Perspectives, Bull. Am. Meteorol. Soc., 83(5), 683–698, doi:10.1175/1520-0477(2002)083<0683:CBESCF>2.3.CO;2, 2002.

Mason, S. J. and Graham, N. E.: Conditional Probabilities, Relative Operating Characteristics, and Relative Operating Levels, Weather Forecast., 14(5), 713–725, doi:10.1175/1520-0434(1999)014<0713:CPROCA>2.0.CO;2, 1999.

Supplementary Figures

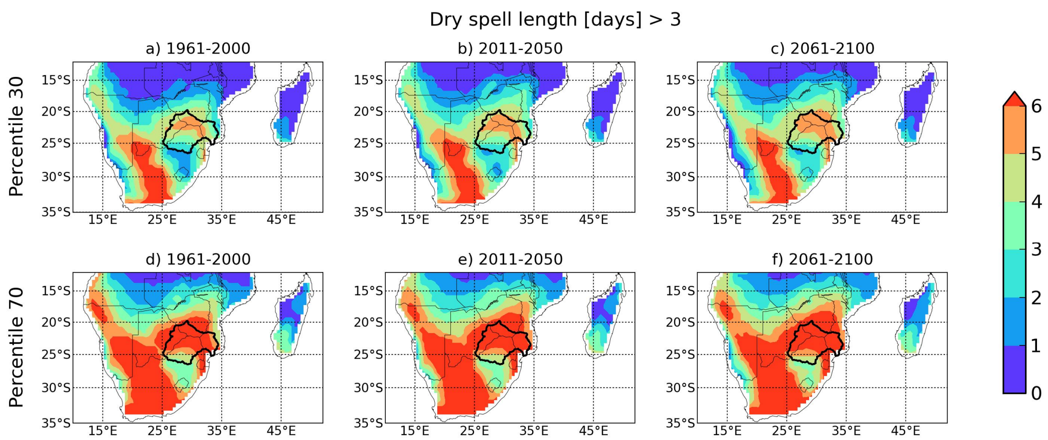

Figure S1. Changes in the climatology of DJF frequency of occurrence of dry spells longer than 3 days. The top row shows the 30 percentile. The bottom shows the 70 percentile. From left to right, the changes in dry-spell frequency climatology are shown along different time slices in the RCM runs (1961-2000, 2011-2050 abd 2061-2100).

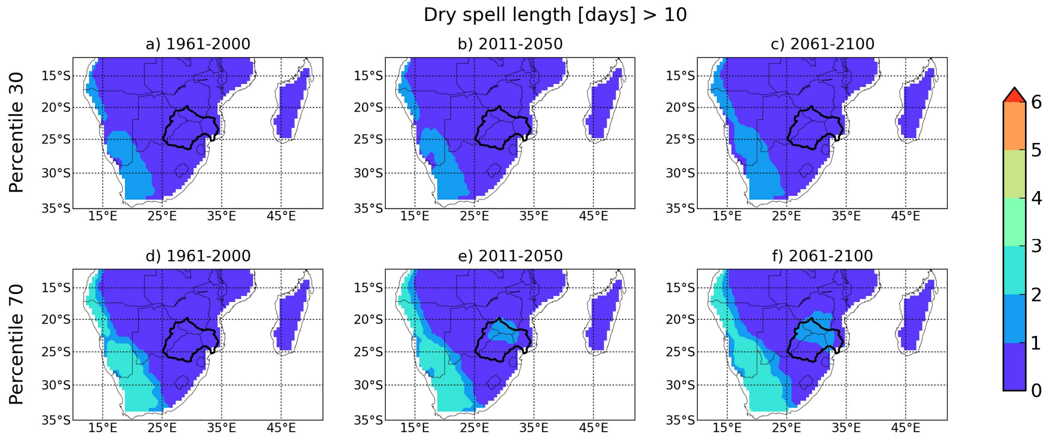

Figure S2. Same as Figure S1 but for changes in the climatology of DJF frequency of occurrence of dry spells longer than 10 days.

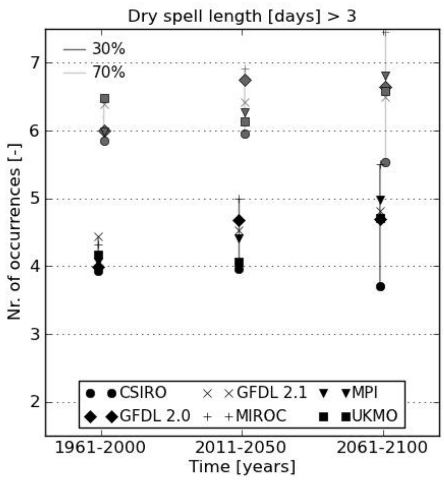

Figure S3. Limpopo basin-averaged changes in climatology from 1961-2000 to 2011-2050 to 2061-2100, of DJF frequency of occurrence of dry spells longer than 3 days according to the 6 RCM projections.

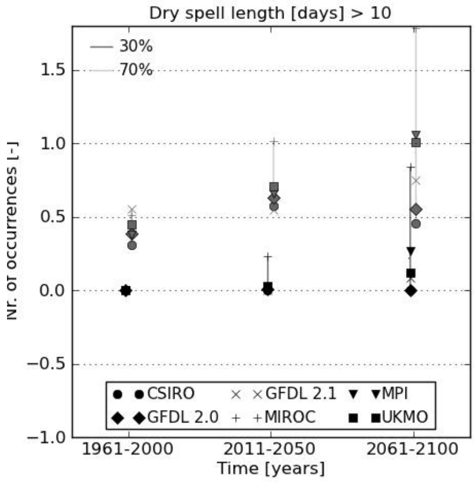

Figure S4. Same as Figure S3 but for changes in climatology of DJF frequency of occurrence of dry spells longer than 10 days.

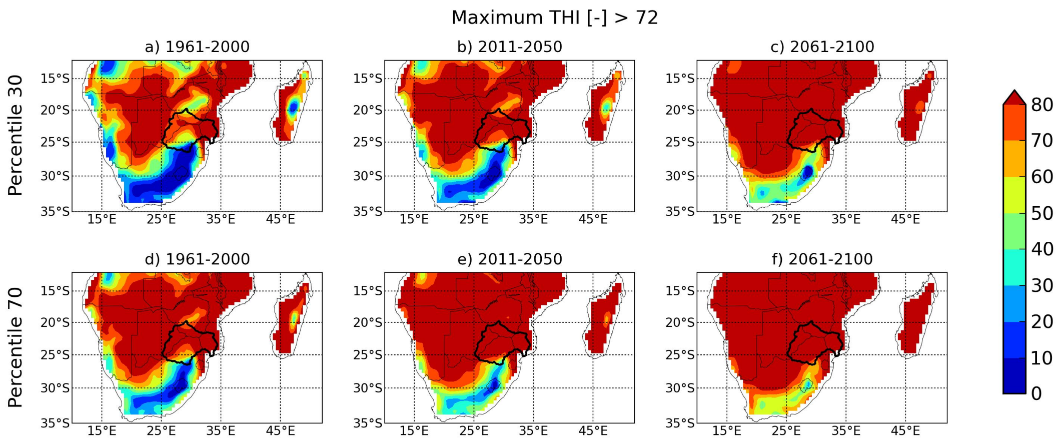

Figure S5. Same as Figure S1 but for changes in the climatology of DJF frequency of occurrence of days with THI higher than 72.

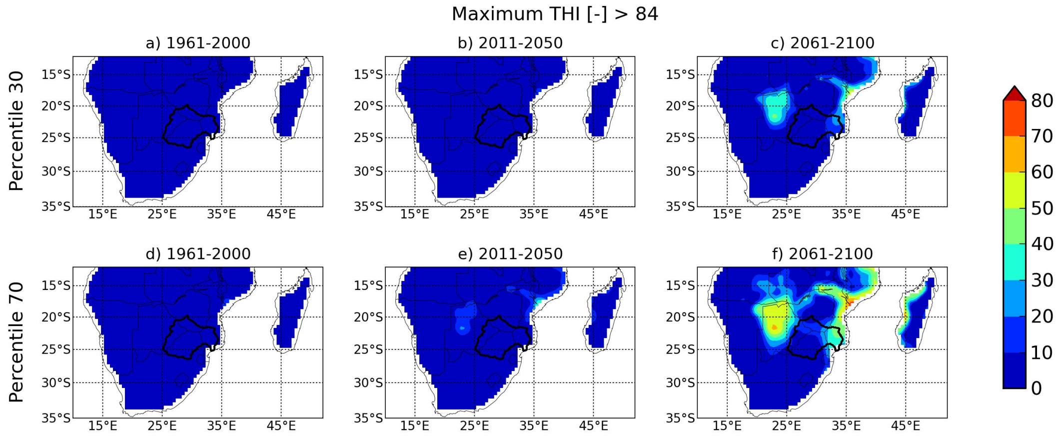

Figure S6. Same as Figure S1 but for changes in the climatology of DJF frequency of occurrence of days with THI higher than 84.

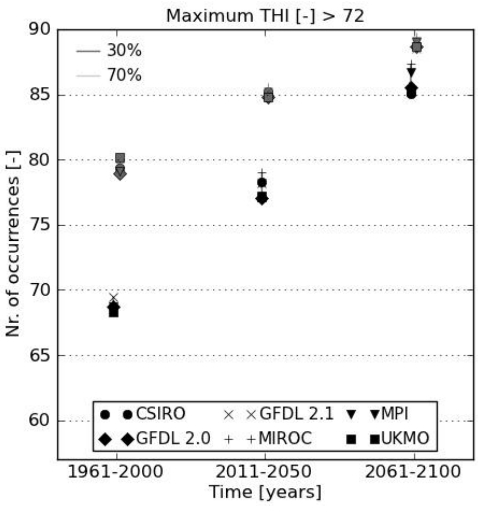

Figure S7. Same as Figure S3 but for changes in climatology of DJF frequency of occurrence of days with THI higher than 72

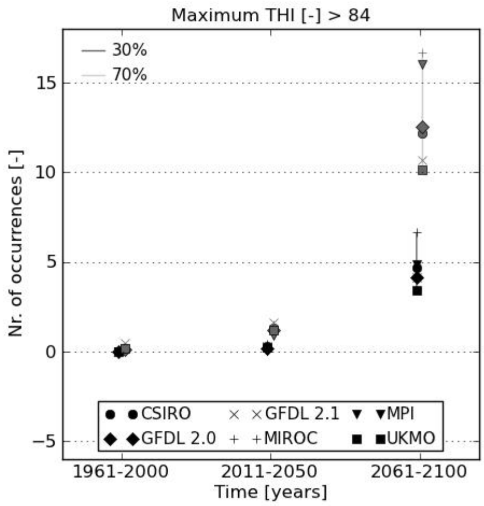

Figure S8. Same as Figure S3 but for changes in climatology of DJF frequency of occurrence of days with THI higher than 84.

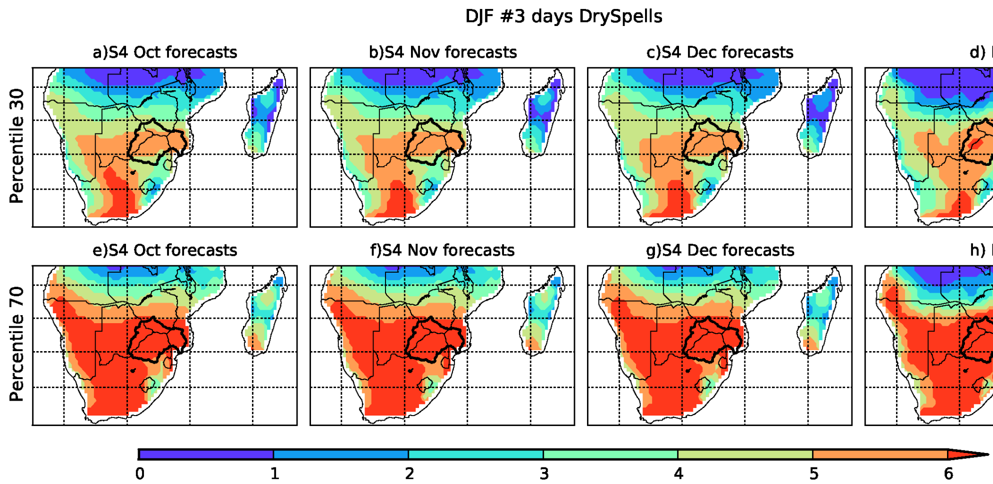

Figure S9. As Figure 4 but for the frequency of occurrence of 3 days dry spells.

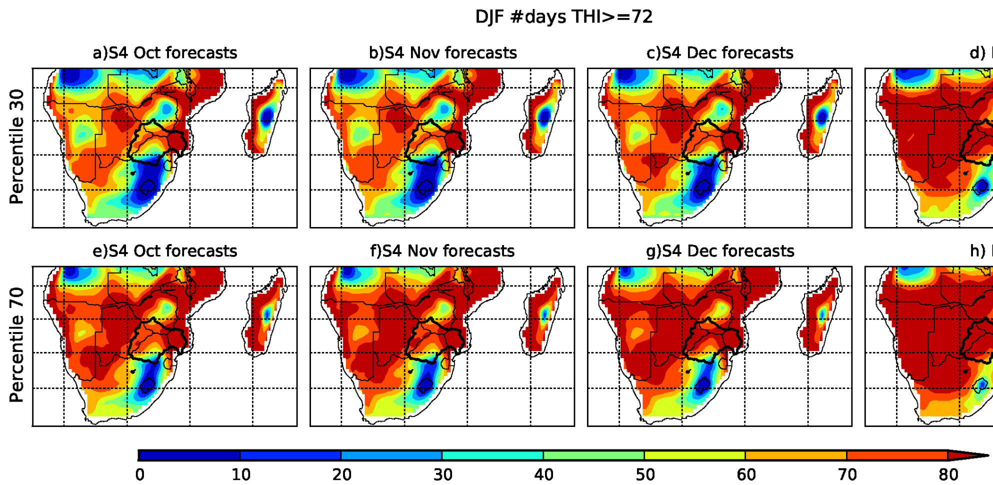

Figure S10. As Figure 5 but for the frequency of occurrence of days with THI higher than 72.

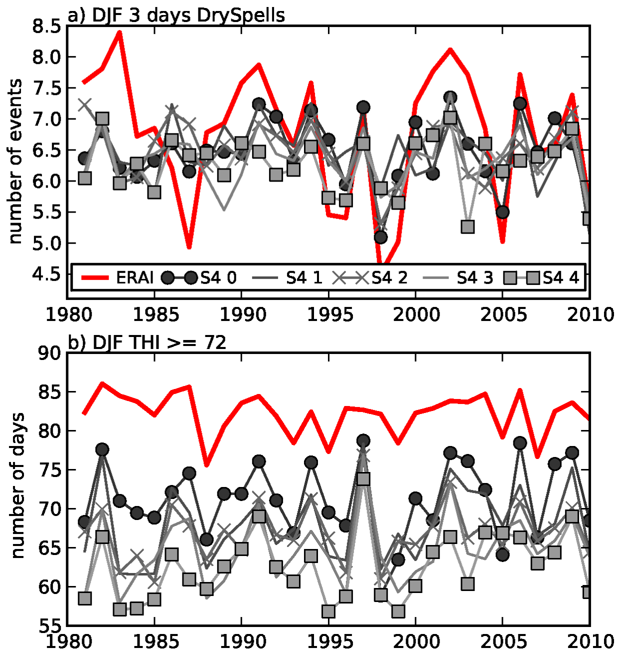

Figure S11. As Figure 6 but for the frequency of occurrences of 3 days dry spells (a) and frequency of occurrence of days with THI higher than 72 (b).

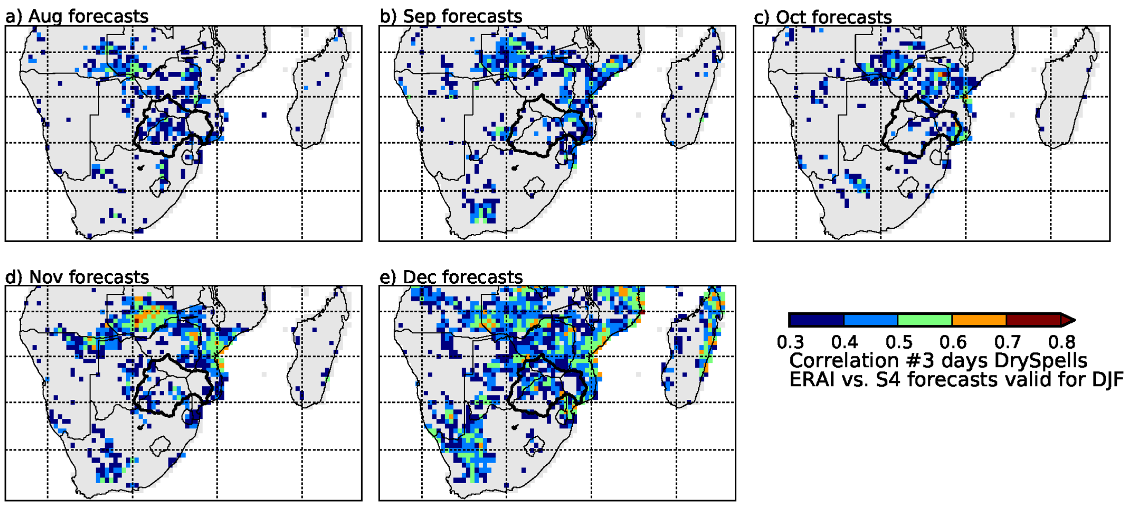

Figure S12. Maps of the grid-point temporal correlation of the frequency of occurrence of 3 days dry spells during DJF between the ECMWF S4 forecasts, at different lead times (each panel) and ERA-Interim. Only correlations significant at 95% (using the Fisher r-to-z transformation) are shown.

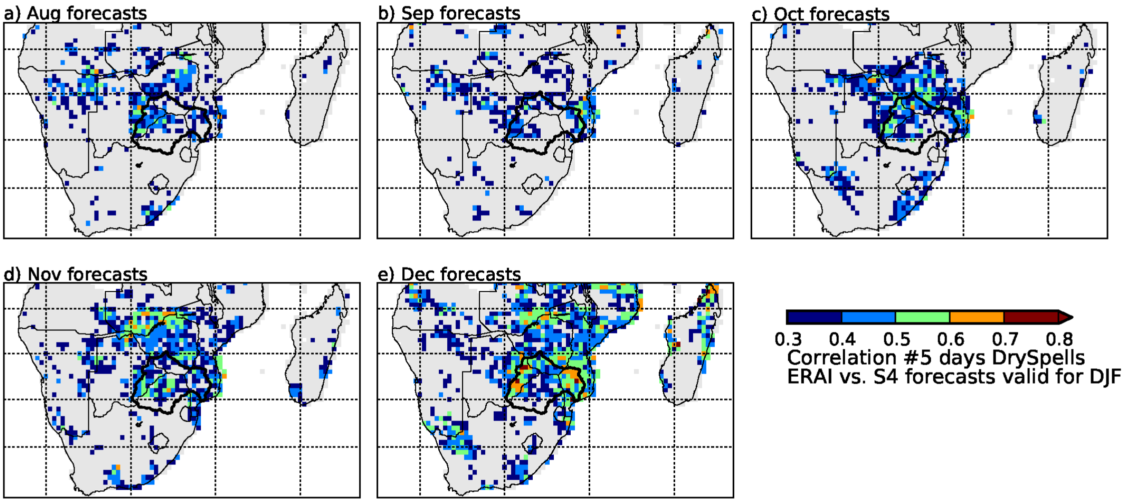

Figure S13. As Figure S12 but the frequency of occurrence of 5 days dry spells.

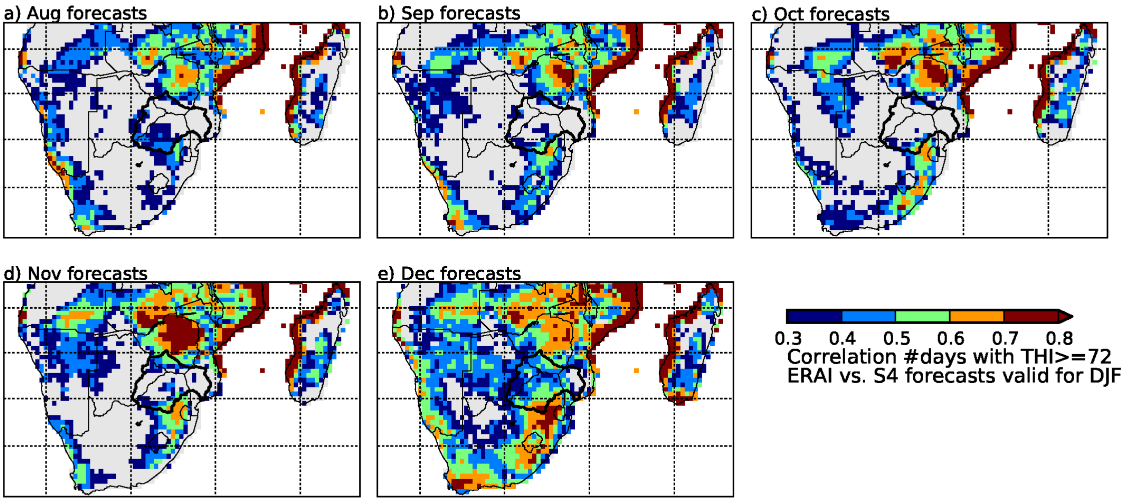

Figure S14. As Figure S12 but for the frequency of occurrence of days with THI higher than 72.

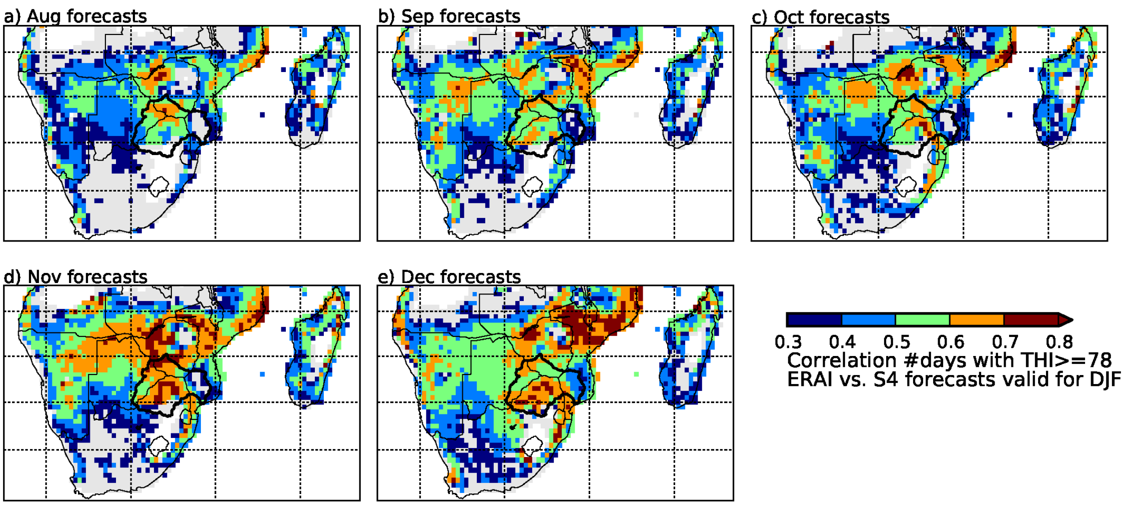

Figure S15. As Figure S12 but for the frequency of occurrence of days with THI higher than 78.

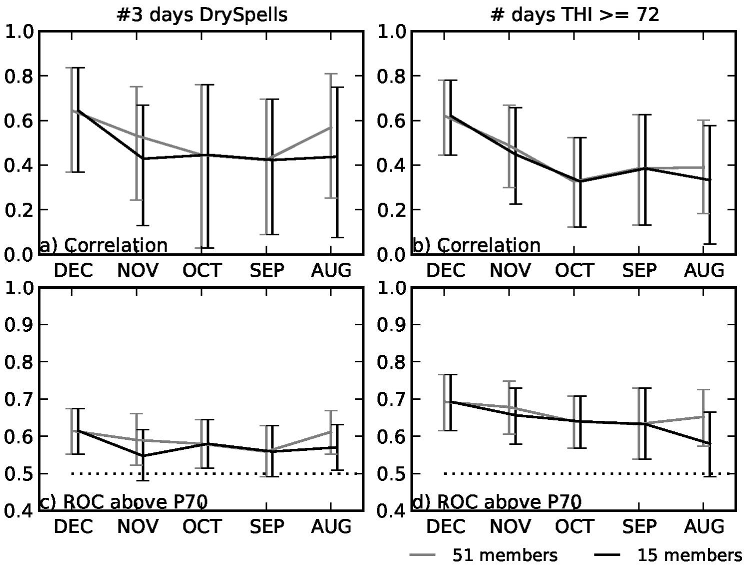

Figure S16. As Figure 7 but for the DJF frequency of occurrence of 3-day dry spells (a,c) and frequency of occurrence of days with THI higher than 72 (b,d).

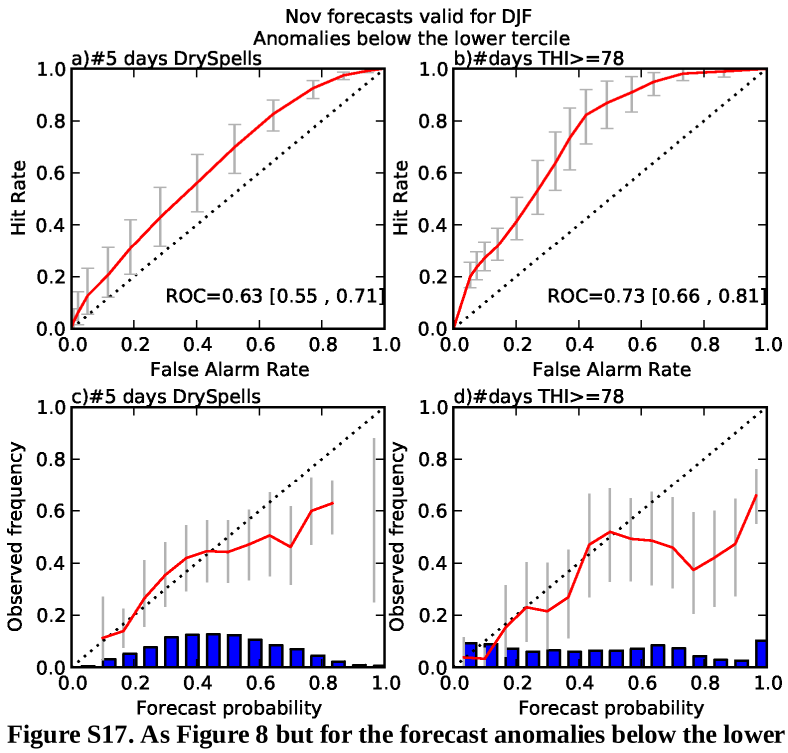

Figure S17. As Figure 8 but for the forecast anomalies below the lower tercile.

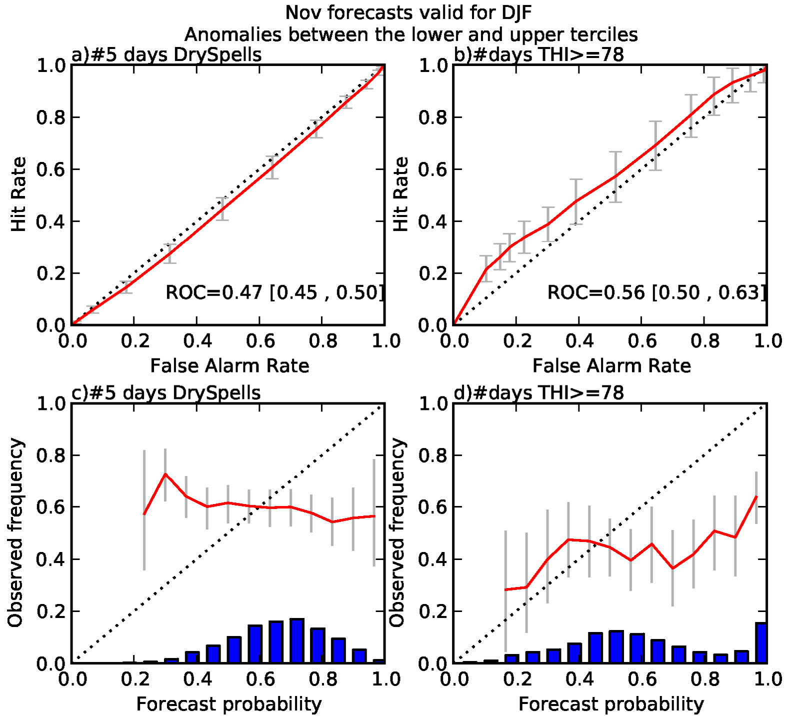

Figure S18. As Figure 8 but for the forecast anomalies between the lower and upper terciles (normal conditions).